

*Geological **F**ield **T**rips and **M**aps*



SOCIETÀ GEOLOGICA ITALIANA

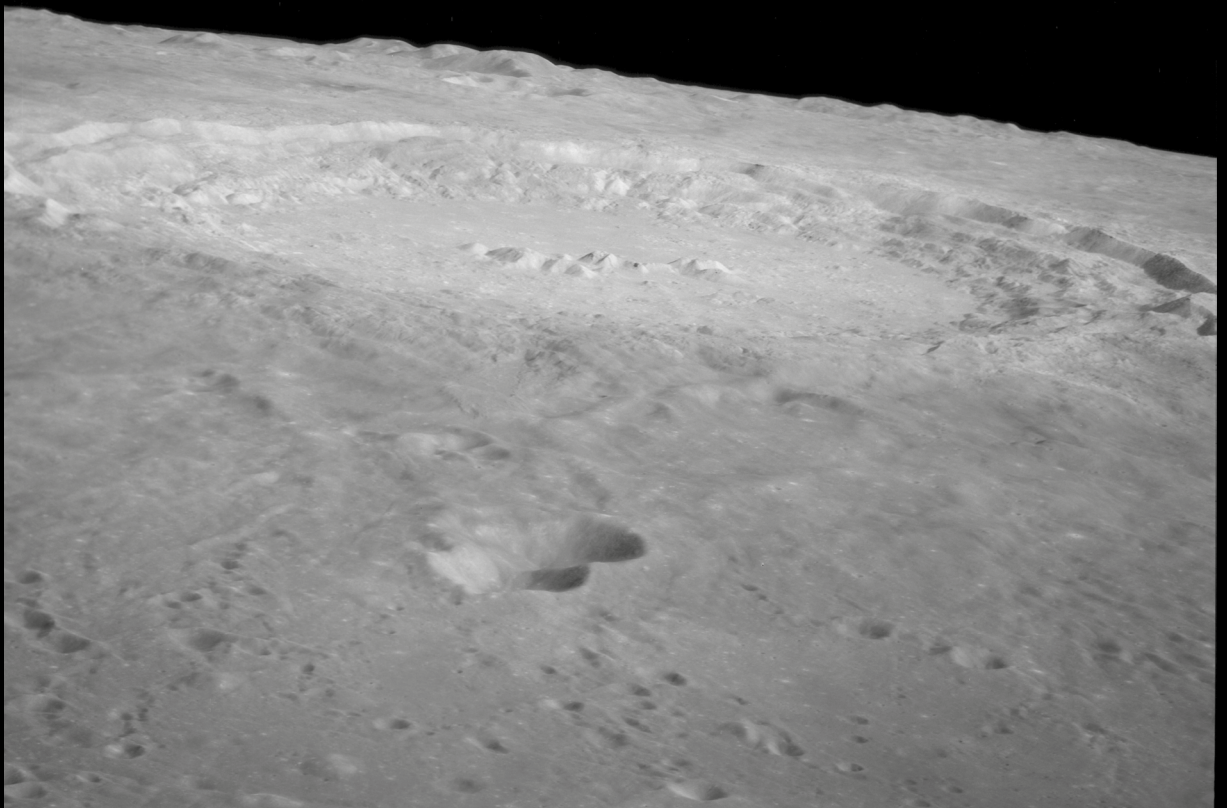
FONDATA NEL 1881 - ENTE MORALE R. D. 17 OTTOBRE 1885



ISPRA
Istituto Superiore per la Protezione
e la Ricerca Ambientale



Sistema Nazionale
per la Protezione
dell'Ambiente



Geologic evolution and map of Copernicus Crater interior (Moon)

<https://doi.org/10.3301/GFT.2024.01>

2024

Vol. 16 (1.1)



ISSN: 2038-4947

GFT&M - *Geological Field Trips and Maps*

Periodico semestrale del Servizio Geologico d'Italia - ISPRA e della Società Geologica Italiana
Geol. F. Trips Maps, Vol.16 No.1.1 (2024), ... pp., ... figs., ... tab., (<https://doi.org/10.3301/GFT.2024.01>)

Geologic evolution and map of Copernicus Crater interior (Moon)

Filippo Tusberti^{1,2}, Matteo Massironi^{1,2,3}, Riccardo Pozzobon^{1,4}, Luca Penasa²

¹ Department of Geosciences, University of Padova, via Giovanni Gradenigo,6, 35131, Padova, Italy.

² INAF-OAPD Astronomical Observatory of Padova, vicolo dell'Osservatorio, 5, 35122, Padova, Italy.

³ CISAS, University of Padova, via Venezia, 15, 35131, Padova, Italy.

⁴ Department of Physics and Astronomy, University of Padova, via Marzolo 8, 35131, Padova, Italy.

Corresponding Author e-mail address: filippo.tusberti@gmail.com

Responsible Director
Maria Siclari (ISPRA-Roma)

Editor in Chief
Andrea Zanchi (Università Milano-Bicocca)

Editorial Manager
Angelo Cipriani (ISPRA-Roma) - *Silvana Falchetti* (ISPRA-Roma)
Fabio Massimo Petti (Società Geologica Italiana - Roma) - *Diego Pieruccioni* (ISPRA - Roma) - *Alessandro Zuccari* (Società Geologica Italiana - Roma)

Associate Editors
M. Berti (Università di Bologna), *M. Della Seta* (Sapienza Università di Roma),
S. Fabbi (Sapienza Università di Roma), *P. Gianolla* (Università di Ferrara),
G. Giordano (Università Roma Tre), *M. Massironi* (Università di Padova),
M.L. Pampaloni (ISPRA-Roma), *M. Pantaloni* (ISPRA-Roma),
M. Scambelluri (Università di Genova), *S. Tavani* (Università di Napoli Federico II)

Editorial Advisory Board
D. Bernoulli, *F. Calamita*, *W. Cavazza*, *F.L. Chiocci*, *R. Compagnoni*,
D. Cosentino, *S. Critelli*, *G.V. Dal Piaz*, *P. Di Stefano*, *C. Doglioni*, *E. Erba*,
R. Fantoni, *M. Marino*, *M. Mellini*, *S. Milli*, *E. Chiarini*, *V. Pascucci*, *L. Passeri*,
A. Peccerillo, *L. Pomar*, *P. Ronchi*, *L.*, *Simone*, *I. Spalla*, *L.H. Tanner*,
C. Venturini, *G. Zuffa*

Technical Advisory Board for Geological Maps
F. Capotorti (ISPRA-Roma), *F. Papasodaro* (ISPRA-Roma),
D. Tacchia (ISPRA-Roma), *S. Grossi* (ISPRA-Roma),
M. Zucali (University of Milano), *S. Zanchetta* (University of Milano-Bicocca),
M. Tropeano (University of Bari), *R. Bonomo* (ISPRA-Roma)

Cover page Figure:

Copernicus crater view looking north. Image captured from lunar orbit during the Apollo 12 mission in 1969.

ISSN: 2038-4947 [online]

<http://gftm.socgeol.it/>

The Geological Survey of Italy, the Società Geologica Italiana and the Editorial group are not responsible for the ideas, opinions and contents of the guides published; the Authors of each paper are responsible for the ideas, opinions and contents published.

Il Servizio Geologico d'Italia, la Società Geologica Italiana e il Gruppo editoriale non sono responsabili delle opinioni espresse e delle affermazioni pubblicate nella guida; l'Autore/i è/sono il/i solo/i responsabile/i.

INDEX

Introduction	4	Crater wall units.....	9
Geologic setting	4	Crater floor's geological units	12
Data	6	Landforms	14
Methods	6	Discussions	14
Mapping and output Scales	9	Conclusions	16
Mapping Workflow	9	References	17
Map description	9		

ABSTRACT

Copernicus is a well-known, almost perfectly circular, complex impact crater with pronounced ejecta rays covering a large part of the lunar near side and for this reason, is used as the stratigraphic base of the Copernican period. Besides its importance to lunar chronostratigraphy, the mineralogical composition of its interior, characterised by an olivine-bearing central peak and compositionally varied floor and inner walls, make this crater particularly interesting for unravelling the nature of both the primordial and deep lunar crust. In addition, the identification of different crater floor materials and features including impact melts, impact breccias, mega-blocks and potential degassing vents within Copernicus are of paramount importance for understanding impact processes and related products. Hence, to foster a future in-situ exploration we have produced a high-resolution geologic map (scale 1:150.000) of the Copernicus crater interior taking into account both geomorphological and spectral information. The morphological analysis was derived mainly from Lunar Reconnaissance Orbiter Camera (LROC), Lunar Orbiter Laser Altimeter (LOLA) and Kaguya Terrain Camera data, whereas the spectral information was retrieved from Clementine data and Kaguya Multiband Imager (MI) spectral maps. Our geological map suggests an oblique impact from the SE with the production of impact melts ejected towards the NW and flowing down on the crater floor covered by impact breccias during the modification stage. The heterogeneous composition of the floor, inner walls and central peaks suggests a variegated shallow and deep lunar crust at the Copernicus impact site.

Keywords: Planetary geology, Copernicus Crater, Moon, Near side, Geologic mapping, GIS.

INTRODUCTION

The renewed interest in Moon robotic exploration missions has become apparent with many recent missions developed by CNSA, ESA, and NASA. CNSA's Chang'e 3 and Chang'e 4 missions have brought two rovers to the lunar surface, the Yutu rover landed in Sinus Iridum in 2013 (Wu et al. 2014; Basilevsky et al., 2015) and the Yutu 2 rover in Von Karman crater at the end of 2018 (Wu et al. 2014). CNSA also realised a sample-return lunar mission thanks to Chang'e 5 (Li et al., 2022). There are several more upcoming robotic and human exploration programs from both NASA and ESA (in the framework of the Artemis program and the Argonaut Logistic Lander respectively; Carpenter et al., 2012), which are closely tied to the heritage of the former Heracles rover exploration mission within the METERON program (Landgraf et al., 2018). In addition, the Japanese private company Ispace has developed the Hakuto mission, which attempted to land the UAE Rashid lander on the lunar surface (Gibney, 2020), whereas the Korean space agency KARI has just successfully launched Korean Pathfinder Lunar Orbiter (KPLO) on August 4, 2022 (Song et al., 2022). In this framework, the accurate geological mapping of potential landing sites is gaining increasing importance, being fundamental for planning missions, observation

strategies, and traverses as well as avoiding potential hazards for landing and roving operations. In particular, understanding the geological evolution of a site of interest provided by a geological map can drive the selection of the scientific targets for any rovers and human exploration.

Copernicus is located on the near side of the Moon and is one of the most important potential targets of lunar exploration (Bugiolacchi et al., 2011; Dhingra et al., 2013; Iqbal et al., 2020). Indeed, after the seminal work on geological lunar mapping of Shoemaker (1961), it was the subject of many studies even during the Apollo missions (Binder and Roberts, 1970), although never selected as a landing site. Studying Copernicus means having the possibility to gather information about the shallow and deep lunar crust both in terms of composition and evolution (Snyder et al., 1992; Elardo et al., 2011) and the impact cratering process (Melosh 1989). Moreover, sampling and dating rocks reset by the impact itself can well constrain the age of a reference stratigraphic plane of the whole Moon with a significant influence on the dating system applied to the entire inner Solar System (Ivanov 2001). This system is indeed based on crater size-frequency distributions and lunar chronological curves (Neukum et al., 2001; Marchi et al., 2009; Le Freuvre and Wieczorek, 2011), constrained on radiometric ages of lunar samples among which the ones from Copernicus ejecta rays have still an uncertain absolute age attribution (Stöffler and Ryder 2001; Iqbal et al., 2020). To foster both the human and robotic exploration and exploitation of this crater, an accurate geologic map illustrating the overall geological evolution of the crater is required. In this work, we produced a geologic map of Copernicus, which aims to improve the previously existing ones (Howard, 1975; Shkuratov et al., 2016) by adding new information, thanks to the availability of more recent and better quality data (both in terms of spectral and spatial resolution) that led to a more in-depth analysis of the geology of the crater. The map presents the geology of the crater's inner walls and floor taking into account both the morphological and spectral characteristics of the different units. It also includes specific landforms such as exposed fault planes, degassing vents, mega-blocks, flow channels and pit chains. The surface composition and landforms revealed by the presented map will highlight the most intriguing potential study targets of Copernicus and its geologic evolution.

GEOLOGIC SETTING

Copernicus (Fig. 1) is a complex impact crater (~96 km in diameter) located just south of the south-western rim of mare Imbrium, on the lunar near side (Min latitude: 8°E; Max latitude 12°E; Dhingra et al., 2013). This crater is relatively

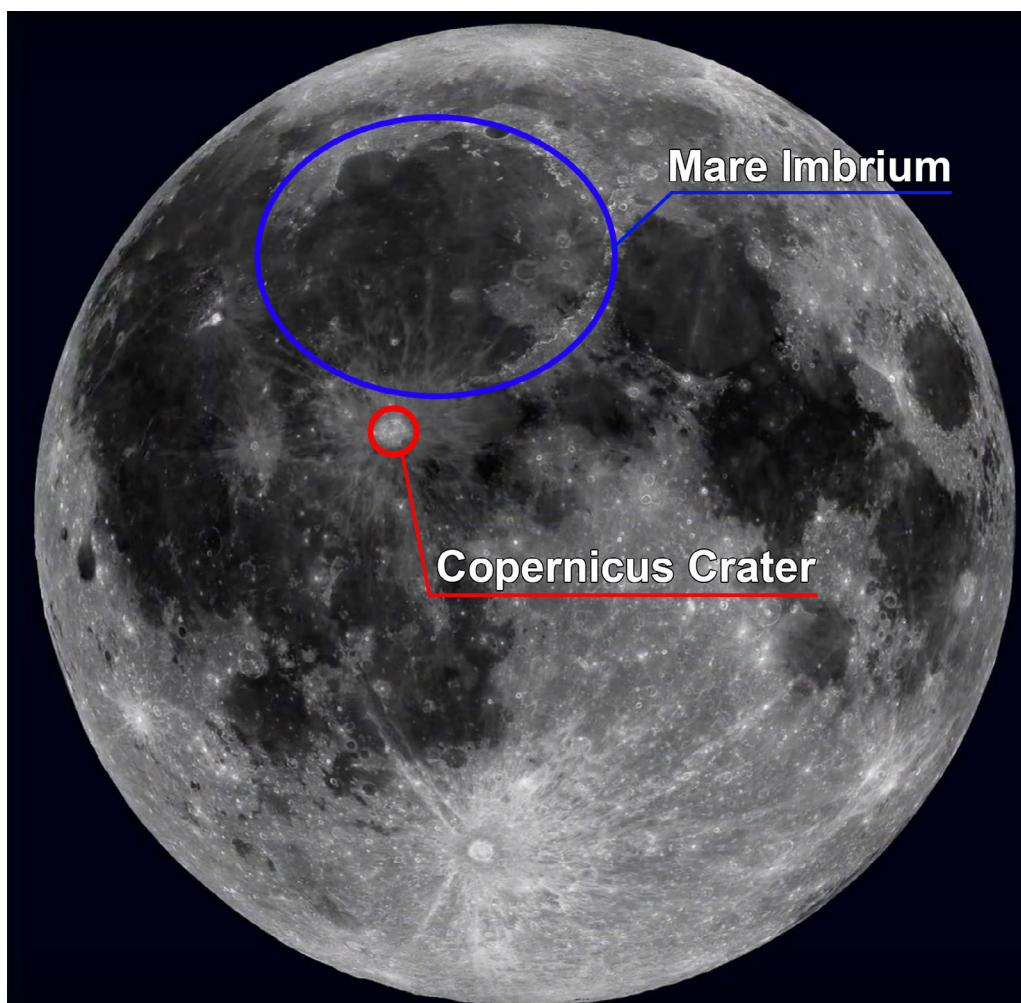


Fig. 1 - Image of the lunar near side (NASA, October 20, 2017), on which the location of Copernicus crater (red) and Mare Imbrium (blue) has been highlighted.

young being dated back to ~ 0.8 Ga (Hiesinger et al., 2012; Terada et al., 2020). The final shape of Copernicus, which has a depth of approximately 3.6 km, is a consequence of classic impact and post-impact modification processes. It presents an almost circular shape, a central peak, a flat floor, and well-developed inner wall terraces (Wood and Anderson, 1978). The target area on the lunar surface where the Copernicus crater was formed, is characterised by elevated terrains, peaks, valleys, and grooves filled with Mare-like materials (Bugiolacchi et al., 2011). Overall, this region is stratigraphically complex and heterogeneous at the boundary between the Procellarum Smooth plains, and Carpatu Mountains corresponding to the Imbrium rim (Fortezzo et al., 2020). The Procellarum is the biggest basin on the Moon containing more than 60% of the lunar maria. It shows diverse units of different ages, and an extreme variety of geologic structures such as prominent complex craters, ridges, and volcanic domes (Hiesinger et al., 2003; Andrews-Hanna et al., 2014). The Imbrium basin has a diameter of around 1115 km and is the second largest lunar mare (Warren and Wasson 1979; Warren, 1985; Jolliff et al., 2000). The rim and the walls of Copernicus are characterised by extensive slumps of rock material, along with concentric

normal and listric faults, whose presence is highlighted by well-developed scarps and terraces (Howard, 1975). A certain compositional difference has been documented on local spectral signatures of the crater's inner walls showing an increasing depth of the clinopyroxene absorption bands from the northern rim to the southern one (Bugiolacchi et al., 2011). In addition, several studies have shown the presence of olivine in the lower part of the northern inner wall (e.g., Chevrel et al., 1991; Lucey et al., 1991; Sprague et al., 1992; Le Mouélic and Langevin, 2001; Yamamoto et al., 2010; Pinet et al., 2018).

The crater floor surrounding the central peaks has a generally flat topography, but with several areas showing rough and hummocky morphologies, suggesting the presence of complex sub-melt layer topography. The hummocky areas cover 3/4 of the crater floor, whereas the northwest quarter appears smoother and flatter. Most of Copernicus' smooth floor appears finely pitted, suggesting that an intense debris fall of melt-rich materials could have occurred at the end of the cratering process (Bugiolacchi et al., 2011). These were likely ejected at a high angle and fell back into the crater before the melt veneer was solidified (Dence, 1971; Hawke and Head 1977). Indeed, the shocked and brecciated floor

materials appear to be overlaid by a relatively thin, dark, and uniform sheet of impact material (Warrel et al., 2004). The floor is also rather heterogeneous from the spectral point of view. The southern sector of the rim, the inner wall, and the floor tend to be enriched in clinopyroxenes compared to the northern one (Bugiolacchi et al., 2011). All of this might indicate a more gabbroic composition of the southern sector with respect to the northern one, which is instead more in line with noritic/olivine-noritic rock materials. On the other hand, Shkuratov et al. (2016) interpreted the thermal spectral variegation at the NW quadrant of both the rim and the floor of the Copernicus crater as associated with impact melts and ejecta resulting from an impact onto a formerly heterogeneous crust, including differentiated intrusive bodies of potential dacitic/rhyolitic composition. The central peak is comprised of uplifted deep-seated material which includes olivine-rich bodies (Pieters et al., 1982; Lucey et al., 1991; Sprague et al., 1992; Pinet et al., 1993; Mouélic and Langevin 2001; Warrel et al., 2004; Yamamoto et al., 2010; Liu et al., 2011; Dhingra et al., 2015; Pinet et al., 2018). The central peak is quite uniform both in morphology and albedo and its surface rock texture suggests a highly fractured rock mass from which detached material forms gravitational taluses with accumulation debris at their base.

DATA

To analyse the morphology of the crater, we used data from the LROC-Lunar Reconnaissance Orbiter Camera (Robinson et al., 2010) and LOLA-Lunar Orbiter Laser Altimeter (Smith et al., 2010) both mounted on the Lunar Reconnaissance Orbiter, as well as data from the Terrain Camera of the SELENE-Kaguya mission (Haruyama et al., 2008). In particular, we derived the topographic information from the LOLA and Kaguya combined Digital Elevation Model (DEM; Barker et al., 2016; available on the USGS website), that have a horizontal resolution of 512 pixels per degree (~59 m/px at the equator) and vertical accuracy approximately 3 to 4 m. From this DEM we derived two base maps useful for morphological interpretation: a hillshade with an azimuth of 315° and an altitude of 45°, (Fig. 2a), and the colour-coded Elevation Map (Fig. 2b). In particular, the LROC-WAC (Wide Angle Camera), which acquires colour and ultraviolet images over the complete lunar surface at a spatial resolution of ~100 m/px, (Fig. 2c) was used in combination with the hillshade data, for the interpretation of the general geology of Copernicus, and to map the main geologic units. We used the LROC-WAC Global Morphology Mosaic, developed by the LROC team, at 643 nm. Presenting a spatial resolution of ~0.5 m/px, LROC-NAC (Fig. 2d) (Narrow-Angle Camera) images were very useful

during the mapping process, to clear up doubts about morphologies of some areas and to identify various kinds of landforms like faults, cracks, open pits, pit chains, and flow channels.

We also made extensive use of multispectral data, by using the Clementine UVVIS Warped Colour Ratio Mosaic (Fig. 3a). The global map was generated from UVVIS mosaics using three spectral filters: 415nm, 750nm, and 1000 nm, (Archinal et al., 2005; Hare et al., 2008). The Clementine mosaic is traditionally displayed as an RGB false colour composition with the following band ratios: Red = 750/415 nm; Green = 750/1000 nm; and Blue = 415/750 nm. Following Lucey et al. (2000) (see also Denevi et al., 2008) the red colour represents a high 750/415nm ratio, indicating low titanium or, most probably, high glass contents of the analysed materials, indeed a lower albedo and a higher spectral slope between 750 and 415 nm are usually related to the electronic field effect of Fe oxides (in contrast to the TiO content), the glass content and the presence nFe particles as space weathering effects (Bell et al., 1976; Fischer and Pieters, 1994; Hapke, 2001). In our specific case, where impact materials dominate, high red colours are likely to be interpreted as glassy components from impact melt sheets scattered across the crater floor (Pinet et al., 1993). The green colour represents a high 750/1000nm ratio highlighting the absorption bands induced by iron in silicate minerals (Clark et al., 1957) and thus indicates a higher content of mafic minerals (Wells and Hapke, 1977). The blue colour, instead, represents a high 415/750nm ratio, so a higher titanium content or alternately, bright slopes and albedos that are not compensated by using the image ratios. Yellow-Green areas are due to the combined effect of the amount of mafic minerals (green) and glass content derived by space weathering and/or within impact melts (more likely) (red).

Finally, we used the spectral maps derived from the Kaguya Lunar MI (Ohtake et al., 2008; Ohtake et al., 2013; Lemelin et al., 2016) displaying the percentage content of plagioclase (Fig. 3b), clinopyroxene (Fig. 3c), olivine (Fig. 3d), and orthopyroxene (Fig. 3e). Both the Clementine colour composite and the Kaguya Lunar MI maps were used for the distinction between different spectral sub-units among the same geo-morphological units (Fig. 3f).

METHODS

We distinguished the geological units of Copernicus crater based on their morphologies, textures, colours in Clementine RGB, and stratigraphic relationships. On top of that, we carried out a further distinction of spectral sub-units on the base of the relative mineralogical content derived from the Kaguya Lunar MI maps. Hence, differently from

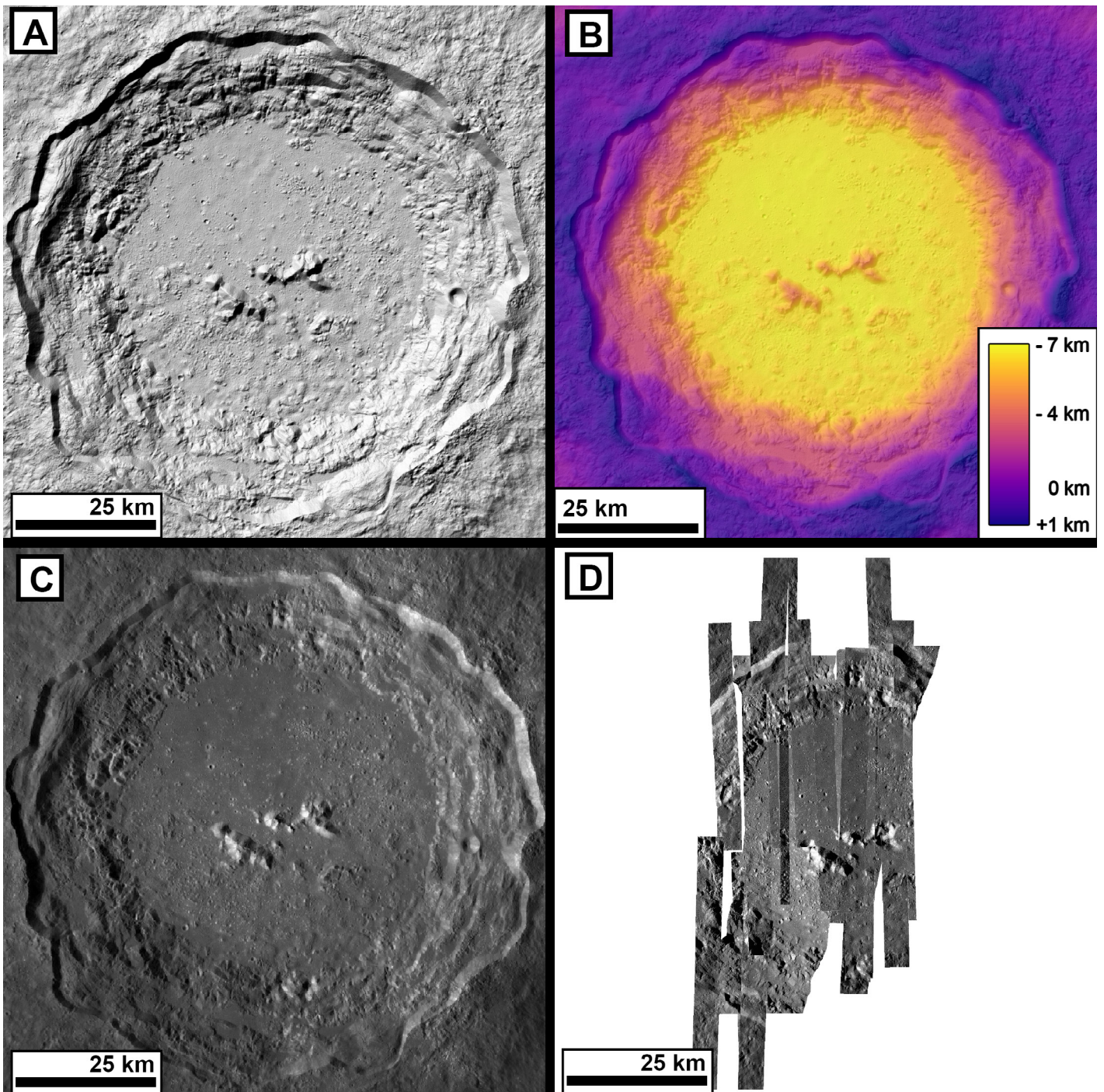


Fig. 2 - a) LRO-WAC: Panchromatic channel with a spatial scale of 100m/px. b) LROC-NAC: high resolution images with a spatial scale of 0.5m/px. b) Hillshade (Az: 315.0; Alt 45.0) generated using the LOLA and Kaguya DEM. c) Hillshade overlaid by coloured LOLA and Kaguya DEM, the deep purple colour is the highest elevation (1695m), the yellow the lowest (-7412m). d) Clementine multispectral data, overlies the hillshade. Red = high 750/415nm, Blue = high 415/750nm, and Green high 750/1000nm.

the previous maps (Howard, 1975; Shkuratov et al., 2015) exclusively based on geomorphological photointerpretation, our geological map also takes into account the spectral differences among the units.

The geologic map uses a cylindrical lunar Equirectangular Projection on the lunar datum (Hargitai et al., 2017) as a system of reference and the hillshade made from LOLA and Kaguya combined DEM as basemap of the final output

map. We generated the map using ArcGIS 10.8, QGIS 3.16 and finally Photoshop CC for the last adjustment of the map output.

The geological cross-section was derived from the topography of the LOLA Kaguya merged DEM and by projecting the geological contacts onto the topographic profile using the “qprof” plugin for QGIS. The geologic interpretation of the section has taken into account the

overlapping/cross-cutting relationships of the units within the crater and the listric fault planes corresponding to the steep scarps of the crater rim likely formed during the impact modification stage.

Mapping and output Scales

In choosing the mapping and output scales we followed USGS guidelines where it is suggested to draw contacts at a scale four to five times larger than the scale of the final output map (Skinner et al., 2018). In addition, we applied the Tobler (1987) rule which defines the maximum mapping scale (S_m) as:

$$S_m = R_r \times 2000$$

where R_r is the raster resolution.

The raster resolution of our mapping basemap ranged between 0.5 m/px of the LROC-NAC images, 59m/px of the hillshade derived from LRO LOLA and Kaguya DEM, and to a lesser extent, 100m/px of the LROC WAC images. Those basemaps led to a maximum potential mapping scale ranging between 1:1.000 and 1:118.000. We finally mapped at a scale between 1:40.000 and 1:100.000. Our output scale of the map is thus 1:150.000 and the wide range of maximum mapping scale lets us generate a map focused on the main general geology of Copernicus, but with significant detail of the features like faults, cracks, open pits, pit chains, and flow channels.

Mapping Workflow

We chose to organise the work in a unique geodatabase, containing a unique feature dataset. Within the dataset, are included three feature classes: *geologic contacts* (i.e., polyline layer), *linear features* (i.e., polyline layer), and *geological units* (i.e., polygon layer).

We started to map from the *geologic contacts* feature class, following the guidelines by (Galluzzi et al., 2016). In short, we have first drawn the contacts of all units and then, only during the mapping finalisation processes. We then converted those contacts into polygons using the “construct polygon” tool of the advanced editor of ArcGIS. In this work, we used only “certain” and “approximate” types of contacts, the first in case of the clear and sharp contrast between different terrains, features, or units; and the second when the contact is gradual or presumed, or its location is not confidently identified because of the data quality (i.e., not an adequate spatial resolution, or under shadows). We used “certain” contacts to map the boundaries of Copernicus’ wall and floor, between the part of the central peaks and other surrounding units. More in general, we used “certain” contacts to define the boundaries

of all the units clearly distinguished from the surrounding morphologies like gentle scarps and terraces, steep scarps, melt pools, some degassing features, and lobate flows and channel materials. On the contrary, we used “approximate” contacts to map gradual or barely defined boundaries because of gradual changes in morphologies, textures and spectra, shadowed areas, and bad quality of the data set on specific locations. In particular, “approximate” contacts are the ones distinguishing units and spectral sub-units of the crater floor (i.e., geological units of smooth floor materials and hummocky floor materials), as well as some boundaries with surrounding morphological features. *Linear features* represent all the morpho-structural features drawable with a line (e.g., faults, fractures, and pit chains). Within this feature class, there is also the feature open pit mapped as a closed-ring linear feature for better map rendering. *Geological units* are the major units of the whole Copernicus crater and were identified using both spectral and morphological data.

MAP DESCRIPTION

The final mapping result is a geological map of the Copernicus crater interior at a scale of 1:150.000. Here, we identified a total of 16 geologic units and 6 landforms divided into these two main categories: *geological units* and *landforms*. We split the first category into two subgroups called *crater floor units* and *crater wall units*. The *crater floor units* represent all the units located inside the floor of Copernicus including the units of the central peak. The *crater wall units* represent all the units between the rim and the floor of the Copernicus crater. Finally, we considered the *landforms* as particular features, both linear and areal, located within the whole Copernicus area. They are not properly geologic units although deeply correlated with many of them (e.g., flow channel landform with lobate flow or channel material unit and open fractures landform with degassing features).

Being all the geological units of the Copernican age, we avoided labels referring to their age and instead favoured labels derived by their names eventually followed by a lowercase suffix for spectral sub-units. For better comprehension of the geologic units’ characteristics and contents, see the summary Tab. 1 and Tab. 2.

Crater wall units

The first-order differentiation of the crater wall units has been made on the base of slope inclination and morphology. We mapped all the areas with a slope range between 8° - 43° as *terrace and gentle scarp* (GS) unit (Fig. 4a). Conversely, we mapped as *steep scarp* (SS) unit the areas steeper than 43° (Fig. 4a), being this angle slightly higher than the lunar

Table 1 - Summary table of the geologic units and their descriptions based on the morphologic observations and Clementine RGB data.

UNIT	ROUGHNESS	CLEMENTINE RGB	CLEMENTINE (nm)	TiO2	GLASS	MAFIC/OL
SFa	Low	Yellow	High 750/415 High 750/1000	Low	High	High
SFb	Low	Bright Red	High 750/415	Low	High	Low
SFc	Low	Variable	-	-	-	-
TS	Mid-Low	Red-Blue	Average 750/415	Mid-Low	Mid-High	Low
TH	Mid-High	Blue-Red	Average 415/750	Mid-High	Mid-Low	Low
HFa	High	Variable	-	-	-	-
HFb	High	Bright Blue	High 415/750	High	Low	Low
CPo	-	Bright Green	High 750/1000	Low	Low	High
CP	-	Variable	-	-	-	-

Table 2 - Summary table showing the percentage weight (%) value of olivine, orthopyroxene, clinopyroxene, and plagioclase of the geologic units.

UNIT	Ol. wt %	OPX wt%	CPX wt%	PLG wt%
GS	~3	15 ÷ 45	~15	50 ÷ 75
GSa	5 ÷ 10	~0	0 ÷ 15	88 ÷ 93
SS	~3	15 ÷ 45	~15	50 ÷ 75
SSa	5 ÷ 10	~0	0 ÷ 15	88 ÷ 93
SFa	~3	15 ÷ 40	5 ÷ 15	73 ÷ 78
SFb	~8	~0	0 ÷ 15	88 ÷ 93
SFc	0 ÷ 10	15 ÷ 40	5 ÷ 30	60 ÷ 77
TS	~4	0 ÷ 15	0 ÷ 15	85 ÷ 90
TH	~4	0 ÷ 15	0 ÷ 15	80 ÷ 88
HFa	0 ÷ 5	15 ÷ 30	0 ÷ 15	55 ÷ 77
HFb	0 ÷ 5	~10	0 ÷ 15	80 ÷ 86
CPo	9 ÷ 20	~0	0 ÷ 7	80 ÷ 90
CP	5 ÷ 11	~0	0 ÷ 10	85 ÷ 92

regolith angle of repose (40°ca., Carrier et al. 1991) and well above the more frequent slopes of taluses and gravitational deposits on the Moon (31-34°, e.g., Kokelaar et al., 2017). We then found spectral subunits. Kaguya MI spectral maps evidenced in most of the inner wall (southern and eastern sector), a content in plagioclase of 50 ÷ 75%, a content of 15 ÷ 45% in orthopyroxene (Fig. 4b), and a content of ~15% in clinopyroxene (GS and SS units). Those contents are more in line with the composition of the surrounding surface (at a regional scale) than the northwest sector. Indeed, that specific area seems to be covered by ejecta extremely rich in plagioclase (88 ÷ 93%) and glass (Fig. 4c), and extremely poor in orthopyroxene (~0%). Following that difference in composition, we distinguished these sub-units with different colours and added the suffix “a” at the end of

the name and the related label: *terrace and gentle scarp a* (GSa) and *steep scarp a* (SSa; Fig. 4a).

Lobate flow and channel materials (LC) are located in the lower half of the crater wall (Fig. 4a). These landforms are characterised by lobes and channels most probably due to downhill flows of viscous partially molten material (i.e., impact melts; Howard, 1975). Those features, show a textured morphology composed of sub-parallel corrugations and ponds and sometimes terminate with a melt pool at their base.

Melt pool (MP) unit shows smooth and flat-shaped areas, often surrounded by a rough and corrugated morphology (Fig. 4a). Some melt pools are present also within the floor of the crater but are too small to be effectively mapped at the output scale of the map (i.e., 1:150.000).

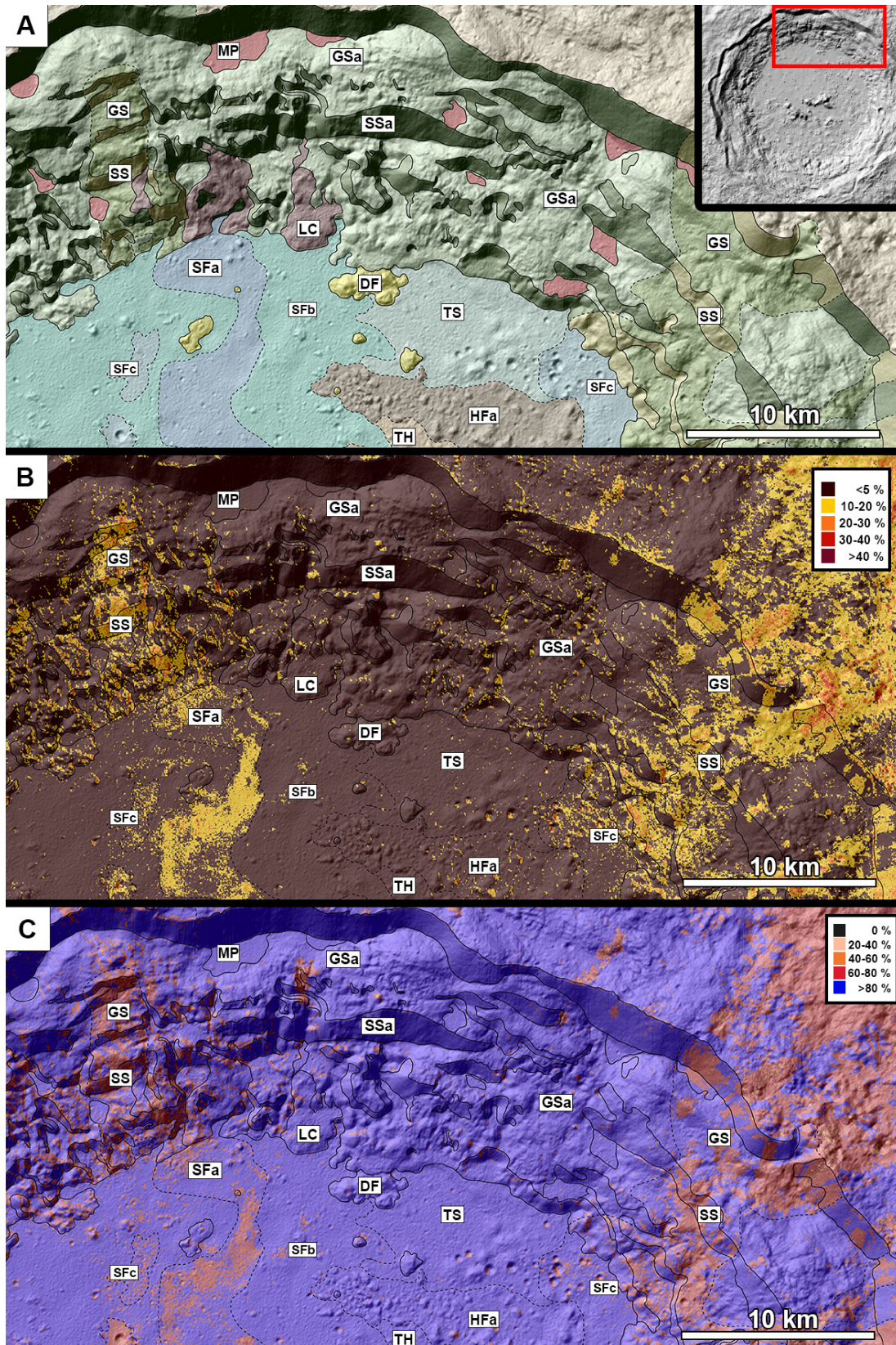


Fig. 4 - a) A closeup of the northern part of Copernicus wall, showing the geologic units and subunits mapped: terrace and gentle scarp (GS, GSa) and steep scarp (SS, SSa), lobate flow or channel material (LC), melt pools (MP), smooth floor material (SFa, SFb, SFC), degassing features and related deposits (DF), transitional smooth material (TS), transitional hummocky material (TH), and hummocky floor material a (HFa). In order to highlight the differences in orthopyroxene and plagioclase content between the units GS and GSa, and SS and SSa, we represent the same area but where colours indicate a content of (b) 15÷45% (wt) in orthopyroxenes, and (c) 88÷93% (wt) in plagioclase.

Crater floor's geological units

The floor of Copernicus crater (Fig. 5a), with the only exception of the outcropping central peak, is filled by *smooth floor materials* (SF), mainly distributed on the northwestern quadrangle, and *hummocky floor materials* (HF), covering especially the southern sector. In between these two main units are transitional geological units of variable degrees of roughness named *transitional smooth materials* (TS) or *transitional hummocky materials* (TH). The general arrangement of the units and their contacts suggest that the *smooth materials* (SF) gradually overlap the hummocky ones (Fig. 5a). The SF and the HF units are spectrally distinct and a certain variability in the composition is also apparent within

each unit. This allowed us to distinguish sub-units from the main ones. The entire series of floor units are cut and overlapped by *degassing features and related deposits* (DF). In the following, we will describe each unit in more detail.

The *smooth floor material* (SF) unit is characterised by a high smoothness on the crater floor displaying a very low amount of blocks and mounds. Despite its morphological uniformity, this unit shows spectral variations visible both on Clementine and Kaguya MI data, displayed by 3 subunits in apparent stratigraphic sequence: SFa, SFb, and SFc.

The sub-unit *smooth floor material a* (SFa) is characterised by distinct spectral properties and sinuous boundaries. [Dhingra et al. \(2013\)](#) interpreted this geological body as a heterogeneous impact melt feature, enriched in Mg-pyroxene. Kaguya MI spectral maps confirmed the enrichment of the sub-unit in orthopyroxene (15% ÷ 40%). They also highlight a lower content of plagioclase (73% ÷ 78%) and olivine (~3%) with respect to the SF unit (Fig. 5b). This sub-unit is thought to be at the top of the entire sequence of smooth materials.

Smooth floor material b (SFb) is the most extensive smooth floor subunit and is stratigraphically positioned just below the SFa unit. On Clementine data, it shows a bright red colour (Fig. 5c) and is characterised by a high 750/415nm ratio indicating a low TiO₂ and/or a high glass content, whereas the Kaguya maps highlight a very high value in plagioclase (88% ÷ 93%), almost void orthopyroxene value and very low clinopyroxene amount (~0% ÷ 15%; Fig. 5b). In addition, the olivine content is generally very low (~8%).

The *smooth floor material c* (SFc) shows approximately the same content of orthopyroxene and plagioclase of the SFa unit, but it is also enriched in clinopyroxene (~5% ÷ 30%). The SFc unit underlies the SFb unit being often exposed in correspondence of small craters and related ejecta onto the SFb unit. Considering the crater depth/diameter ratio relation by [Stopar et al. \(2017\)](#), we calculated the excavation depth of each crater that exposed the SFc unit. The shallowest one is 30 m and the deepest one is 200m (Tab. 3), this means that SFc top is at 30m in depth and extends up to at least 200 m in depth.

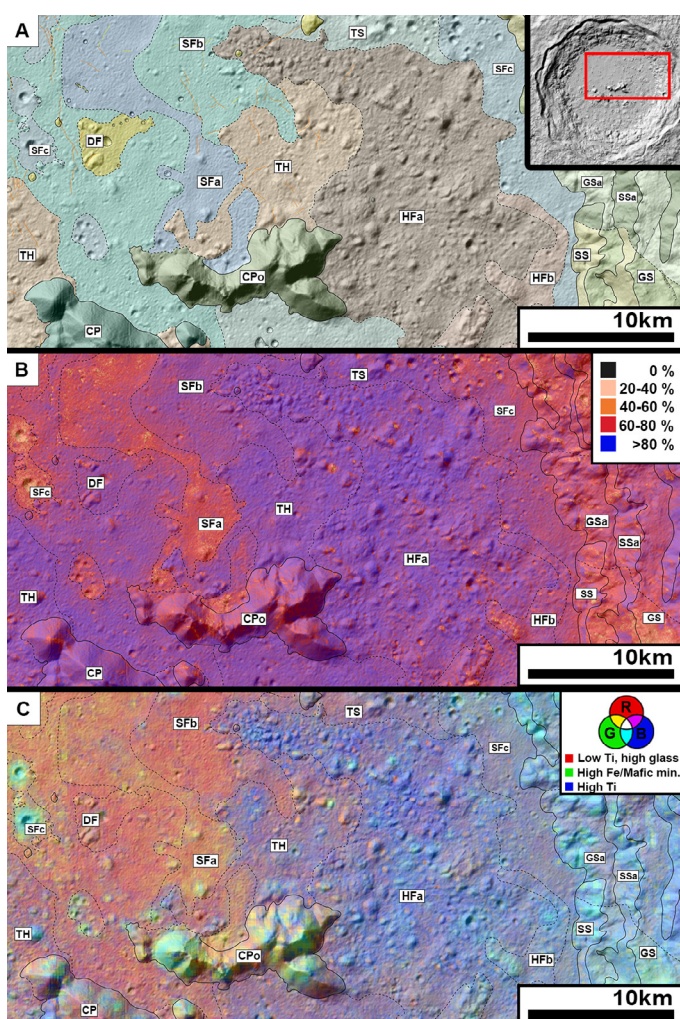


Fig. 5 - A close-up of the (a) geological units mapped within the floor of Copernicus: smooth floor material (SFa, SFb, SFc), hummocky floor material (HFa, HFb), transitional smooth material (TS), transitional hummocky material (TH), degassing features and related deposits (DF), central peak material (CP), and olivine-rich central peak material (CPo). Additionally, terrace and gentle scarp (GS, GSa) as well as steep scarp (SS, Ssa) units are also present. The same area and corresponding units are further shown by their (b) plagioclase weight percentage content, and their (c) Clementine RGB false colour composition .

Table 3

Crater (n°)	Ratio d/D	Diameter D (m)	Calculated Depth d (m)
1	0.21	870	183
2	0.21	950	200
3	0.17	380	65
4	0.17	390	66
5	0.17	300	51
6	0.17	400	68
7	0.17	275	47
8	0.21	550	116
9	0.15	200	30

The *hummocky floor material* (HF) unit has the highest roughness among the floor units, it shows abundant blocks and mounds and a homogeneous morphology. Nevertheless, there are two distinct spectral hummocky floor subunits, visible both on Clementine and Kaguya MI data: HFa and HFb

On Clementine images, *hummocky floor materials a* (HFa) shows a bright blue colour (Fig 5c) due to its high value of the 415/750 nm ratio interpreted as an enrichment of TiO₂ and/or a shortage of glass content. Moreover, Kaguya MI shows low orthopyroxene (~10%) and clinopyroxene content (~0% ÷ 15%), and a very high amount of plagioclase (80% ÷ 86%). The sub-unit *hummocky floor materials b* (HFb) is visible in Kaguya MI spectral maps where it is evidenced by a higher content of orthopyroxene (15% ÷ 30%) and a lower content in plagioclase (55% ÷ 77%) with respect to HFa (Fig 5b).

The *transitional smooth materials* (TS) unit is characterised by mid-low roughness due to dispersed blocks and mounds. In contrast, within the *transitional hummocky materials* unit (TH) they are more frequent, hence leading to a mid-high roughness. Clementine data (Fig. 5a) indicates that both two units present average values of 415/750 nm and 750/415nm ratios: TS has a little higher 750/415 nm ratio (more reddish colour on Clementine RGB), whereas TH has a little higher 415/750 nm ratio (more bluish colour on Clementine RGB; Fig. 5c). For a better comprehension of

some characteristics of those features see the summary Tab. 1 and Tab. 2.

The unit *degassing features and related deposits* (DF) consists of vents and small cone to dome-shaped edifices and related ejecta deposits, often surrounded or crossed by cracks. These features and deposits are possibly derived from degassing of vugs and pockets of volatiles within the impact melts of the smooth floor and hummocky materials. Alternatively, they can be interpreted as vents, cinder cones, and pyroclastic material derived from local explosive volcanism. However, being not associated with any specific spectral signatures with respect to the surrounding materials, the volatiles degassing seems to be a more reliable interpretation, despite some cone-shaped landforms strictly resembling cinder cones.

The Copernicus crater is characterised by an articulated central peak which we have divided into two units: the *central peak material* (CP) and the *olivine-rich central peak material* (CPo; Fig. 6a), both characterised by scree or talus at their base. The CP unit, represented by the southernmost peak, doesn't show any significant spectral signature both in Clementine and Kaguya spectral data except for a very high value of plagioclase (85% ÷ 92%; Fig. 6b). On the contrary, the CPo unit is the northernmost peak and, on Kaguya spectral maps, shows a massive enrichment in olivine (up to ~20%; Fig. 6c). On Clementine data, a high

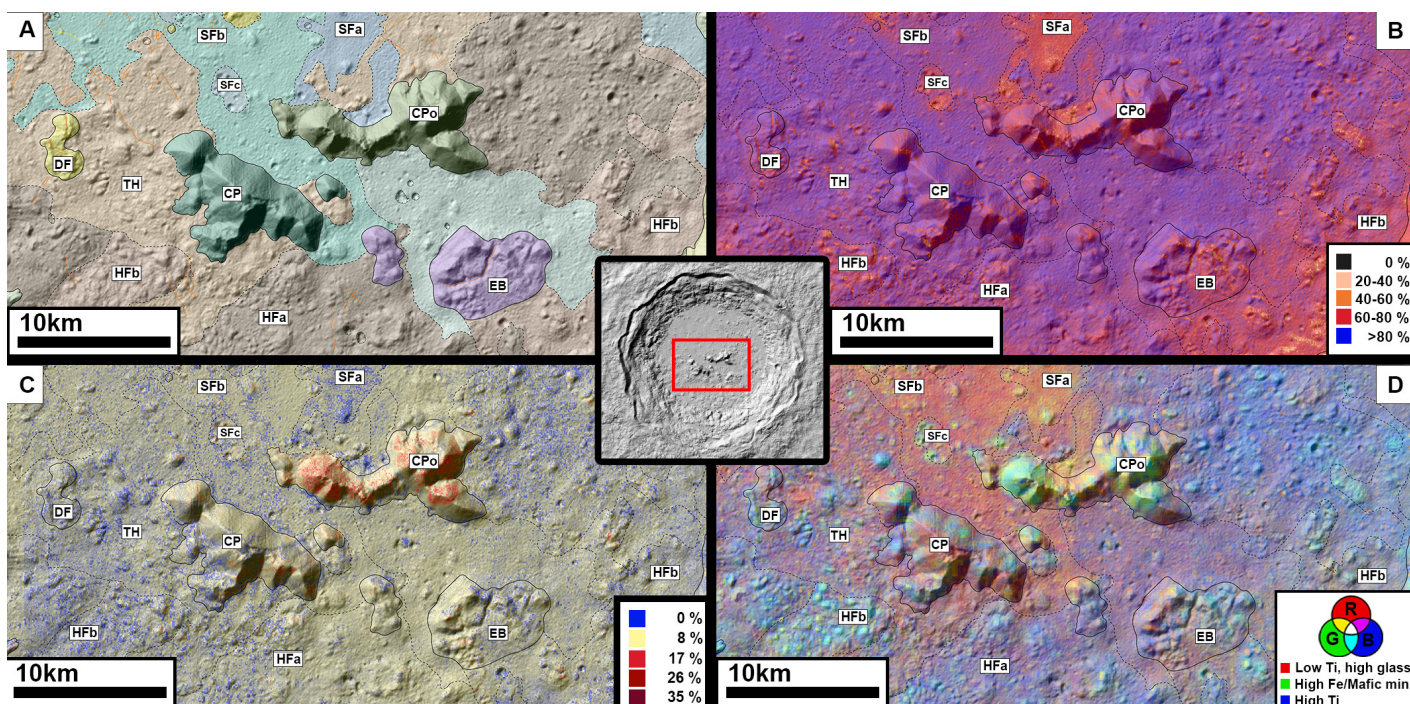


Fig. 6 - A close-up of the central peak area of Copernicus, showing the units present in this area: smooth floor material (SFa, SFb, SFc), hummocky floor material (HFa, HFb), transitional hummocky material (TH), degassing features and related deposits (DF), megablock ejecta (EB), central peak material (CP), and olivine-rich central peak material (CPo). This figure reveals the clear difference in composition between the CPo and CP units. a) Geological units mapped. b) Weight percentage of plagioclase content in the central peak area. c) Weight percentage of olivine content in the central peak area. d) Clementine RGB colour composition.

ratio 750/1000 nm, might indicate a significant content of Fe in the olivine solid solution (Fig. 6d). Kaguya MI spectral maps also show a slightly lower plagioclase content with respect to the CP unit (Fig. 6b; Tab. 2).

Landforms

We have distinguished different landforms on the crater floor and on the crater rim and inner walls. Most of the landforms in the floor are related to degassing and fracturing processes whereas the wall is dominated by faulting and inward impact melt flows.

The *open pit* landforms in the crater floor (Fig. 7a) are indeed circular depressions without any raised rim indicating their endogenic origin through degassing of trapped volatiles within the impact melt (more probable) or sudden post-impact evacuation of still-molten fallback (Howard, 1975). Some of them show degassing deposits inside and in the surroundings giving rise to the Df unit. In some places, the open pits are organised in *pit chains* represented by lines of open pits and are often associated with other degassing features like vents or fractures.

Open fractures within the crater floor represent irregular open fractures (Fig. 7b), caused by the rapid cooling of the floor's veneer during the formation of the crater (Morris et al., 2000), or potentially related to degassing processes.

We also mapped *ejecta megablocks* (EB) which are groups of large and fractured ejecta blocks, with a variable colour in Clementine RGB composition and no particular compositional variations highlighted by the Kaguya MI spectral data.

Rim and wall faults are the faults that bound the horst and graben systems characterising the entire inner wall. We used the *flow channel* linear feature to indicate the interpreted direction of the downhill flows pertaining to the *lobate flow and channel materials unit* (LC). Finally, we have also indicated the unmapped areas surrounding Copernicus as *surrounding terrains* (TT). These areas consist of the

continuous ejecta of Copernicus located just outside of the crater.

DISCUSSIONS

Our new geological map of Copernicus crater improves, with compositional information and high-resolution details, the previous ones which were produced at a lower scale and mainly based on geomorphological observations (Binder and Roberts, 1970; Howard, 1975; Fortezzo et al., 2020) with limited compositional inferences (Shkuratov et al. 2016). Although the overall results are in line with previous hypotheses, our main findings have highlighted the following points:

- the dichotomous character of the Copernicus crater floor is both morphological and compositional. In particular, the NW sector is a smooth region generally characterised by a high content of plagioclase (>80%) and a higher content of olivine and glass than the rest of the crater floor. Indeed, glassy material is clearly expected within fast-cooled impact melts, which are likely representative of the smooth units (SFa, SFb, Sfc). Nevertheless, there are localised smooth subunits (SFa and Sfc) which show some spectral variation with respect to the more extended one SFb. Indeed, they contain up to ~15% of orthopyroxene and ~20% less plagioclase than the SFb subunit. Whereas SFa clearly overlaps SFb, the larger impact craters on SFb seem to excavate material with the same spectral composition as Sfc which hence underlies SFb. Using the depth of those impact craters, we also calculated that Sfc occurs between 30 m to at least 200m constraining the thickness of unit SFb to <30m and Sfc like material to > 170m. The other sectors of the crater floor are dominated by hummocky materials (HFa, HFb) generally characterised by higher titanium and

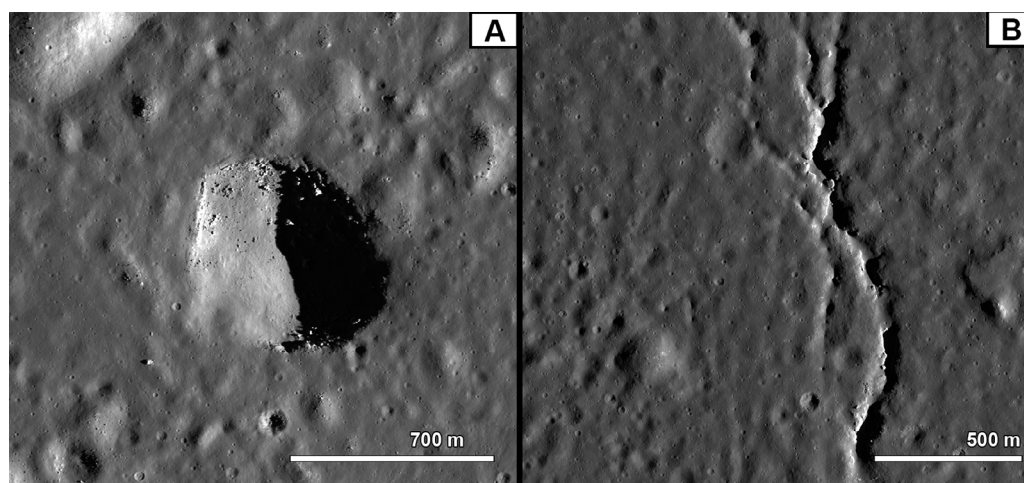


Fig. 7 - a) LROC-NAC data close-up images of an open pit and b) a fracture, both located into the northwestern quadrant.

lower glass content with respect to the smooth units. They also show a higher amount of orthopyroxene, and a lower amount of plagioclase with respect to the SFb subunit, being more similar to the SFa and SFc. The smooth floor units clearly overlie the hummocky ones through a gradational contact encompassing two units with intermediate morphological and compositional characters (TS and TH). Subunits of the smooth material indicate a compositional variability of the impact melts which is likely reflecting the original heterogeneity of the crust before the impact. The higher content of plagioclase (and clinopyroxene) with respect to the hummocky material suggests that the melt may be strongly affected by the anorthositic-gabbroic primordial crust which at the moment of the impact was underlying the basaltic sequence of the Procellarum basin and exposed on the Imbrium rim represented by the Carpatos Mountains. However, considering the orthopyroxene content of SFa and its moderate content in plagioclase it is conceivable a pre-impact crust also containing Mg suite intrusive bodies such as norites.

- The compositional variety of the articulated central peak indicates heterogeneity of the deep crust as well. In particular, the northernmost peak mountain is characterised by evident olivine content which might indicate the exhumation of deep troctolitic/dunitic bodies.
- The compositional dichotomy of the floor is equally reflected on the rim and inner wall which is instead uniform from the geomorphological point of view. In particular, the northern sector seems to be generally enriched in plagioclase, olivine, and glass, whereas it shows a lower content of orthopyroxene. On the contrary, the southern sector more likely has a higher content of orthopyroxene, and lower content of plagioclase and glass. The fan-shaped outward distribution of the material with the same composition as the north-west crater floor sector (i.e., high glass, plagioclase and olivine, and low orthopyroxene) and the frequent impact melt flows mainly characterising the northern inner wall, suggest that the compositional variability on the rim and inner wall is due to an asymmetric distribution of the ejecta blanket covering a substantially uniform substratum constituting the entire inner walls.
- The degassing forms and deposits do not show any compositional variability with respect to the surrounding suggesting that these features may be generated by the releasing of volatiles trapped within impact melt voids, at the time of the crater's formation.

The shape of the craters can remain circular for impacts with angles above 10-15°, but the eccentricity of the

impact on the ejecta can still be observed even at angles ranging between 40-30° (Gault and Wedekind, 1978; Bottke et al., 2000; Kenkmann et al., 2014). Despite Copernicus having a circular shape, Shkuratov et al. (2016) highlighted that the distribution of the striated ejecta around the crater is not homogeneous being extended predominantly on the NE and SW quadrants. All these points depict the Copernicus as resulting from an oblique impact coming from the SE. In the case of an oblique event, the increase of pressure and temperature at the contact stage is asymmetrically distributed and would account for a predominant production of impact melt on the NW side (Pierazzo and Melosh 2000; Kenkmann et al., 2014; Melosh et al., 2016). During the following excavation stage, the melt was mainly ejected towards the NW and in the modification, stage flowed down covering the impact breccias fallen within the crater floor. This stratigraphic sequence is indeed common within several complex impact craters on Earth and other Terrestrial bodies (e.g., Osinski et al. 2011; Osinski and Grieve, 2016; Grieve and Theriault, 2016). The gas trapped within voids in the melt was afterwards expelled producing degassing features and ejecta as envisaged already by Howard (1975). The different glass content between the NW sector and the remaining sectors of the crater floor is directly reflecting the amount of the impact melt within the smooth floor. The different content in orthopyroxene and plagioclase on the northern inner wall and the southern one can be likely explained by ejecta and melts covering the northern sector, being the southern one instead more intermixed with materials of the lunar upper crust at the site of the Copernicus crater (i.e., Ti-rich basalts of the Procellarum maria). This is indeed proven by the higher glass content on the northern inner wall which is likely related to the impact melt mantling the wall itself. The high content of plagioclase (and clinopyroxene) in the glass-dominated smooth floor units suggest that the excavation was able to reach the gabbro-anorthositic primordial crust underneath the Procellarum basalt infilling or involve the same crust exposed along the Carpatos Mountains to the northeast.

The difference between the northwestern sector and the rest of the crater may be led by a pre-existing heterogeneity of the target at the moment of the impact, which occurred in the Montes Carpatos area (Spudis et al., 1993). The area was most probably characterised by highlands units with an irregular topography that formed mounds and valleys. This area was partly overlaid by the maria material (Bugiolacchi et al., 2011) likely coming from the Procellarum maria, most probably leaving partly exposed older highland ridges. The impact might have hit those irregularities and eventually ejected the highland material toward the NW (the downrange direction) whereas the impact breccia and

melt of the mare material could have been ejected in the other direction. The melt generated on both sides flowed downward during the modification stage and gradually draped the floor.

On the bases of Thermal Infrared data, [Shkuratov et al. \(2016\)](#) suggest that the area was affected also by felsic bodies within the pre-impact crust. However, the high content of clinopyroxene and plagioclase puzzles this view with the only exception of the SFa unit where the high content of orthopyroxene and the moderate content of plagioclase point towards a potential presence of Mg suite bodies in the pre-impact crust. In this case, mangerites or charnokites together with norites could be much more likely rather than the rhyolites and dacites suggested by [Shkuratov et al. \(2016\)](#). Some olivine-rich spots on the northern wall and in the SFa unit might instead indicate the sporadic presence of troctolites.

The presence of two central peaks with different composition further suggests a heterogenous target being the olivine-rich northern peak (Fig. 3d) likely representative of a deep crust with troctolitic intrusive bodies.

CONCLUSIONS

The Copernicus impact crater is one of the most coveted lunar targets because it is one of the youngest lunar complex craters on the near side and its absolute age is still uncertain, although used to calibrate the chronological curve for crater density dating of planetary surfaces. To encourage the upcoming lunar exploration missions and to explore the Copernicus crater, accurate geologic cartography of this area is required in the attempt of clarifying the impact process responsible for its geological evolution.

We produced a geologic map of Copernicus, based on the geology and composition of the whole complex crater interior, at a scale of 1:150.000. The geological map is accompanied by a geological section explaining the structural and stratigraphic relationship among units. The map includes units and features that have been distinguished through morphological, stratigraphic, and spectral/colour information. Morphological data have been derived from LOLA and Kaguya DEM, hillshade, LROC-WAC, and LRO-NAC. Whereas spectral/colour data from Clementine UVIS Warped Colour Ratio global mosaic and Kaguya Lunar MI. Combining that information, a total of 16 units have been found and mapped.

The hummocky units, are thought to cover the whole floor, being gradually draped by the smooth units, especially in the north-western quadrant. The composition between hummocky and smooth units is distinct with a higher amount of glass on the latter interpreted as impact melts. The transition between the two terrains is marked by units with transitional morphological and compositional characters. The inner wall is characterised by steep slopes alternating with gentle terraces and is compositionally heterogeneous being the southern part likely representative of the lunar upper crust pertaining to Procellarum maria and the northern part covered by ejecta dominated by impact melts which partly flowed down towards the floor during the impact modification stage. All the observations, illustrated in the geological map, indicate an oblique impact coming from the SE and able to produce and eject towards the NW abundant impact melts. The compositional heterogeneity of the different geological units within the floor, including the central peak, suggests an upper crust mainly composed of the Procellarum Maria basalt, a lower crust characterised by intrusive bodies of different composition pertaining to the highlands and the eventual uplift of deep crustal levels.

This study, coupled with the geological map, provides an overview of the geology of the entire Copernicus crater, its composition, dynamics formation, and the potential geology of the pre-impact target. Additional studies focusing on specific sections of Copernicus would be required and the best candidate is the northwestern sector being particularly smooth and thus well suited for landing and traverse planning. Studying the difference between this particular area and the rest of the crater will discriminate if the pre impact target had an extremely heterogeneous composition exposed by the oblique impact. An exploration mission (robotic or human) to Copernicus would let us to better understand the processes that formed the uneven floor and inner walls of this crater as well as its olive bearing central peak and would allow absolute age determinations pivotal for refining crater-size frequency distribution dating.

ACKNOWLEDGEMENTS

This research was supported by the European Union's Horizon 2020 under grant agreement N° 776276-PLANMAP and 871149-EPN2024 (GMAP-RI).

REFERENCES

- Andrews-Hanna J.C., Besserer J., Head III J.W., Howett C.J., Kiefer W.S., Lucey P.J., McGovern P.J., Melosh H.J., Neumann G.A., Phillips R.J., Schenk P.M., Smith D.E., Solomon S.C., Zuber M.T. (2014) - Structure and evolution of the lunar Procellarum region as revealed by GRAIL gravity data. *Nature*, 514(7520), 68-71.
- Archinal B.A., Rosiek M.R., Redding B.L. (2005) - Unified lunar control network 2005 and topographic model. 36th LSPC. Lunar and Planetary Science XXXVI.
- Barker M.K., Mazarico E., Neumann G.A., Zuber M.T., Haruyama J., Smith D.E. (2015) - A new lunar digital elevation model from the Lunar Orbiter Laser Altimeter and SELENE Terrain Camera. *Icarus*, 273, 346-355, <https://doi.org/10.1016/j.icarus.2015.07.039>.
- Basilevsky A.T., Abdrakhimov A.M., Head J.W., Pieters C.M., Wu Y., Xiao L. (2015) - Geologic Characteristics of the Luna 17/ Lunokhod 1 and Chang'E-3/Yutu Landing Sites, Northwest Mare Imbrium of the Moon. *Planet. Space Sci.*, 117, 385-400, <https://doi.org/10.1016/j.pss.2015.08.006>.
- Bottke Jr W.F., Love S.G., Tytell D., Glotch T. (2000) - Interpreting the elliptical crater populations on Mars, Venus, and the Moon. *Icarus*, 145(1), 108-121.
- Bell P.M., Mao H.K., Weeks R.A. (1976) - Optical spectra and electron paramagnetic resonance of lunar and synthetic glasses: A study of the effects of controlled atmosphere, composition, and temperature. *Lunar Planet. Sci.*, VII, 2543-2559.
- Binder A. B. and Roberts D.L. (1970) - Criteria for Lunar site selection. Astro Sciences Center IIT Research Institute Chicago, Illinois, 38 pp.
- Bugiolacchi R., Mall U., Bhatt M., McKenna-Lawlor S., Banaszkiwicz M., Brønstad K., Nathues A., Søråas F., Ullaland K., Pedersen R.B. (2011) - An In-Depth Look at the Lunar Crater Copernicus: Exposed Mineralogy by High-Resolution near-Infrared Spectroscopy. *Icarus*, 213(1), 43-63, <https://doi.org/10.1016/j.icarus.2011.02.023>.
- Carrier W.D. III, Olhoeft G.R., Mendell W. (1991) - Physical properties of the lunar surface. In: Heiken G., Vaniman D., French B.M. (Eds), *Lunar Sourcebook, A User's Guide to the Moon*, 475-594.
- Carpenter J.D., Fisackerly R., De Rosa D., Houdou B. (2012) - Scientific preparations for lunar exploration with the European Lunar Lander. *Planet. Space Sci.*, 74, 208-223, <https://doi.org/10.1016/j.pss.2012.07.024>.
- Chevrel S., Pinet P., Lesbre O. (1991) - Copernicus: Comparison and complementarity between telescopic multispectral solid state imaging and reflectance spectra. *Lunar Planet. Sci.*, XXII, 201.
- Cintala M.J. and Grieve Richard A.F. (1998) - Scaling impact melting and crater dimensions: Implications for the Lunar cratering record. *Meteorit. Planet. Sci.*, 33 (4), 889-912, <https://doi.org/10.1111/j.1945-5100.1998.tb01695.x>.
- Clark Jr S.P. (1957) - Absorption spectra of some silicates in the visible and near infrared. *American Mineralogist: J. Earth Planet. Mat.*, 42(11-12), 732-742.
- Denevi B.W., Lucey P.G., Sherman S.B. (2008) - Radiative transfer modelling of near infrared spectra of lunar mare soils: Theory and measurements. *J. Geophys. Res.*, 113, E02003. <https://doi.org/10.1029/2007JE002929>.
- Dence M.R. (1971) - Impact melts. *J. Geophys. Res.*, 76(23), 5552-5565, <https://doi.org/10.1029/JB076i023p05552>.
- Dhingra D., Pieters C.M., Head, J.W., (2015) - Multiple origins for olivine at Copernicus Crater. *Earth Planet. Sci. Lett.*, 420, 95-101. <https://doi.org/10.1016/j.epsl.2015.03.039>.
- Dhingra D., Pieters C.M., Head J.W., Isaacson P.J. (2013) - Large mineralogically distinct impact melt feature at Copernicus Crater - Evidence for retention of compositional heterogeneity. *Geophys. Res. Lett.*, 40(6), 1043-1048, <https://doi.org/10.1002/grl.50255>.
- Elardo S.M., Draper D.S., Shearer C.K.J. (2011) - Lunar Magma Ocean crystallization revisited: bulk composition, early cumulate mineralogy, and the source regions of the highlands Mg-suite. *Geochim. Cosmochim. Acta*, 75(1), 3024-3045, <http://dx.doi.org/10.1016/j.gca.2011.02.033>.
- Fischer E.M. and Pieters C.M. (1994) - Remote determination of exposure degree and iron concentration of lunar soils using VIS-NIR spectroscopic methods. *Icarus*, 111(2), 475-488, <https://doi.org/10.1006/icar.1994.1158>.
- Fortezzo C.M., Spudis P.D., Harrel S.L. (2020) - Realise of the Digital Unified Global Geologic Map of the Moon at 1:5,000,000-Scale. Paper presented at the 51st Lunar and Planetary Science Conference, Lunar and Planetary Institute, Houston, TX, <https://www.hou.usra.edu/meetings/lpsc2020/pdf/2760.pdf>.
- Galluzzi V.A., Guzzetta L., Ferranti L., Di Achille G., Rothery D.A., Palumbo P.A. (2016) - Geology of the Victoria Quadrangle (H02), Mercury. *J. Maps*, 12(1), 227-238, <https://doi.org/10.1080/17445647.2016.1193777>.
- Gault D.E. and Wedekind J.A. (1978) - Experimental studies of oblique impact. Lunar and Planetary Science Conference, 9th, Houston, Texas., March 13-17, 1978, Proceedings. Volume 3 (A79-39253 16-91) New York, Pergamon Press, Inc., 1978, 3843-3875.
- Gibney E. (2020) - UAE announces first Arab Moon mission. *Nature*, 587(7833), 186-187.
- Grieve R.A. and Therriault A.M. (2016) - Impactites: their characteristics and spatial distribution. In: Osinki G.R. and Pierazzo E. (Eds.), *Impact processes and products*, Wiley-Blackwell, 90-105.
- Hapke B. (2001) - Space weathering from Mercury to the asteroid belt. *J. Geophys. Res.*, 106(E5), 10039-10073, <https://doi.org/10.1029/2000JE001338>.
- Hare T.M., Archinal B.A., Becker T.L., Lee E.M., Gaddis L.R., Redding B.L., Roseik M.R. (2008) - Clementine Mosaic Warped. *Lunar and Planetary Science*, XXXIX 1097. U.S. Geological Survey, 1-2. Retrieved from <http://www.lpi.usra.edu/meetings/lpsc2008/pdf/2337.pdf>
- Hargitai H., Wang J., Stooke P.J., Karachevtseva I., Kereszturi A., Gede M. (2017) - Map projections in planetary cartography. In: Lapaine M. and Usery E. (Eds), *Choosing a map projection. Lecture notes in geoinformation and cartography*. Springer, 177-202, https://doi.org/10.1007/978-3-319-51835-0_7.
- Haruyama J., Matsunaga T., Ohtake M., Morota T., Honda C., Yokota Y., Torii M., Ogawa Y., LISM Working Group (2008) - Global lunar-surface mapping experiment using the Lunar Imager/Spectrometer on SELENE. *Earth Planet. Sp.*, 60, 243-255, <https://doi.org/10.1186/BF03352788>.

- Hawke B.R. and Head J.W. (1977) - Impact melt in Lunar crater interiors. Lunar and Planetary Science Conference, 8.
- Hiesinger H., Head III J.W., Wolf U., Jaumann R., Neukum G. (2003) - Ages and stratigraphy of mare basalts in Oceanus Procellarum, Mare Nubium, Mare Cognitum, and Mare Insularum. *J. Geophys. Res. Planet.*, 108(E7), <https://doi.org/10.1029/2002JE001985>.
- Hiesinger H.V., Van Der Bogert C.H., Pasckert J.H., Funcke L., Giacomini L., Ostrach L.R., Robinson, M.S. (2012) - How old are young Lunar craters? *J. Geophys. Res.*, 117, E00H10, <https://doi.org/10.1029/2011JE003935>.
- Howard K.A. (1975) - Moon geologic map of the Crater Copernicus. Retrieved from <https://astrogeology.usgs.gov/search/map/Moon/Geology/year-1970/Moon-Geologic-Mapof-the-Crater-Copernicus>.
- Ivanov B. (2001) - Mars/Moon cratering ratio estimates. *Space Sci. Rev.*, 96, 87-104, <https://doi.org/10.1023/A:1011941121102>.
- Iqbal W., Hiesinger H., van der Bogert C.H. (2020) - Geological mapping and chronology of lunar landing sites: Apollo 12. *Icarus*, 352, <https://doi.org/10.1016/j.icarus.2020.113991>.
- Jolliff B.L., Gillis J.J., Haskin L.A., Korotev R.L., Wieczorek M.A. (2000) - Major lunar crustal terranes: Surface expressions and crust-mantle origins. *J. Geophys. Res. Planets*, 105(E2), 4197-4216.
- Kenkmann T., Poelchau M. H., Wulf G. (2014) - Structural geology of impact craters. *J. Struct. Geol.*, 62, 156-182.
- Kokelaar B. P., Bahia R. S., Joy K.H., Viroulet S., Gray J.M.N.T. (2017) - Granular avalanches on the Moon: mass-wasting conditions, processes, and features. *J. Geophys. Res.: Planets*, 122(9), 1893-1925, <https://doi.org/10.1002/2017JE005320>.
- Landgraf M., Carey W., Hipkin V., Carpenter J., Hiesinger H. (2018) - HERACLES, Exploring the Moon in an International Context. European Planetary Science Congress, Berlin, Germany.
- Le Freuvre M. and Wieczorek M. A. (2011) - Nonuniform cratering of the Moon and a revised crater chronology of the inner Solar System. *Icarus*, 214(1), 1-20, <https://doi.org/10.1016/j.icarus.2011.03.010>.
- Lemelin M., Lucey P.G., Gaddis L.R., Hare T., Ohtake M. (2016) - Global map products from the Kaguya Multiband Imager at 512 pppd: Minerals, FeO and OMAT, 47th LPSC, abs. #2994, <http://www.hou.usra.edu/meetings/lpsc2016/pdf/2994.pdf>.
- Le Mouélic S. and Langevin Y. (2001) - The olivine at the Lunar Crater Copernicus as seen by Clementine NIR Data. *Planet. Space Sci.*, 49(1), 65-70, [https://doi.org/10.1016/S0032-0633\(00\)00091-X](https://doi.org/10.1016/S0032-0633(00)00091-X).
- Li C., Hu H., Yang M.F., Pei Z.Y., Zhou Q., Ren X., Liu B., Liu D., Zeng X., Zhang G., Zhang H., (2022) - Characteristics of the lunar samples returned by the Chang'E-5 mission. *Natl. Science Rev.*, 9(2), nwab188.
- Liu F., Yang R., Zhang Y., Qiao L., Wang S., Yang Y., Wang X., (2011) - Distribution of olivine and pyroxene derived from Clementine data in Crater Copernicus. *J. Earth Sci.*, 22(5), 586-94, <https://doi.org/10.1007/s12583-011-0209-2>.
- Lucey P.G., Hawke B.R., Horton K. (1991) - The distribution of olivine in the crater Copernicus. *Geophys. Res. Lett.*, 18, 2133-2136.
- Lucey P.G., Blewett D.T., Taylor G.J., Hawke B.R. (2000) - Imaging of Lunar surface maturity. *J. Geophys. Res. Planets*, 105(E8), 20377-20386.
- Marchi S., Mottola S., Cremonese G., Massironi M., Martallato E. (2009) - A new chronology for the Moon and Mercury. *Astron. J.*, 137(6), 4936-4948.
- McCord T.B., Charette M.P., Johnson T.V., Lebofsky L.A., Pieters C., Adams J.B. (1972) - Lunar Spectral Types. *J. Geophys. Res.*, 77(8), 1349-59, <https://doi.org/10.1029/JB077i008p01349>.
- Melosh H.J. (1989) - Impact cratering: A geologic process. Oxford University Press, New York.
- Melosh H.J. (2016) - The contact compression stage of impact cratering. In: Osinski G.R. and Pierazzo E. (Eds.), *Impact processes and products*, Wiley-Blackwell, 32-42.
- Morris A.R., Head J.W., Margot J.-L., Campbell D.B. (2000) - Impact melt distribution and emplacement on Tycho: a new look at an old question. Lunar and Planetary Science Conference, 1828. Retrieved from <https://www.lpi.usra.edu/meetings/lpsc2000/pdf/1828.pdf>.
- Neukum G., Ivanov B.A., Hartmann W.K. (2001) - Cratering records in the inner Solar System in relation to the lunar reference system. *Chronol. Evol. Mars*, 96, 55-86, https://doi.org/10.1007/978-94-017-1035-0_3.
- Ohtake M., Haruyama J., Matsunaga T., Yokota Y., Morota T., Honda C., LISM team (2008) - Performance and scientific objectives of the SELENE (KAGUYA) Multiband Imager. *Earth Planets Space*, 60, 257-264.
- Ohtake M., Pieters C.M., Isaacson P., Besse S., Yokota Y., Matsunaga T. Boardman J., Yamamoto S., Haruyama J., Staid M., Mall U., Green R.O. (2013) - One Moon, many measurements 3: Spectral reflectance. *Icarus*, 226(1), 364-374.
- Osinski G.R. and Grieve R.A. (2016). Comparison of mid size terrestrial complex impact structure: a case study. In: Osinski G.R. and Pierazzo E. (Eds.), *Impact processes and products*, Wiley-Blackwell, 290-305.
- Osinski G.R., Tornabene L.L., Grieve R.A. (2011) - Impact ejecta emplacement on terrestrial planets. *Earth Planet. Sci. Lett.*, 310, 167-181.
- Penasa L., Frigeri A., Pozzobon R., Brandt C.H., De Toffoli B., Naß A., Rossi A.P., Massironi M (2020) - Constructing and deconstructing geological maps: a QGIS plugin for creating topologically consistent geological cartography. *Copernicus Meetings*, EPSC2020-1057, <https://doi.org/10.5194/epsc2020-1057>.
- Pieters C. M. (1982) - Copernicus crater central peak: Lunar Mountain of unique composition, *Science*, 215(4528), 59.
- Pierazzo E. and Melosh H.J. (2000). - Melt production in oblique impacts. *Icarus*, 145, 252-261.
- Pinet P.C., Chevrel S.D., Martin P. (1993) - Copernicus: A regional probe of the Lunar interior. *Science*, 260(5109), 797 - 801, <https://doi.org/10.1126/science.260.5109.797>.
- Pinet P.C., Chevrel S., Daydou Y., Dhingra D. (2016) - Olivine detection and composition determination at Copernicus and Eratosthenes craters. 8th European lunar Symposium 2020, 102-103.
- Pinet P.C., Chevrel S., Daydou Y., Dhingra D. (2018) - Characterization of the olivine/plagioclase mineralogy at Copernicus crater from MGM deconvolution of M3 observations. 49th Annual Lunar and Planetary Science Conference, No. 2083.

- Robbins S.J. (2007) - The scientific context for exploration of the Moon. National Academies Press, <https://doi.org/10.17226/11747>.
- [Robinson M.S., Brylow S.M., Tschimmel M., Humm D., Lawrence S.J., Thomas P.C., Denevi B.W., Bowman-Cisneros E., Zerr J., Ravine M.A., Caplinger M.A. \(2010\) - Lunar Reconnaissance Orbiter Camera \(LROC\) instrument overview. Space Sci. Rev., 150\(1-4\), 81-124, <https://doi.org/10.1007/s11214-010-9634-2>.](#)
- Shkuratov Y., Kaydash V., Rohacheva L., Korokhin V., Ivanov M., Velikodsky Y., Videen G. (2016) - Comparison of Lunar red spots including the crater Copernicus. *Icarus*, 272, 125-139, <https://doi.org/10.1016/j.icarus.2016.02.034>.
- Skinner, J.A., Huff A.E., Fortezzo C.M., Gaither T.A., Hare T.M., Hunter M.A. (2018) - Planetary geologic mapping protocol. Retrieved from <https://planetarymapping.wr.usgs.gov/Page/view/Guidelines>
- Shoemaker E. (1961) - Moon prototype Copernicus geologic map. Retrieved from <https://astrogeology.usgs.gov/search/map/RPIF/Moon/Maps/Copernicus-300>.
- Smith D.E., Zuber M.T., Jackson G.B., Cavanaugh J.F., Neumann G.A., Riris H., Sun X., Zellar R.S., Coltharp C., Connelly J., Katz R.B (2010) - The Lunar Orbiter laser altimeter investigation on the Lunar Reconnaissance Orbiter mission. *Space Sci. Rev.*, 150, 209-241, <https://doi.org/10.1007/s11214-009-9512-y>.
- Snyder G.A., Taylor L.A., Neal C.R. (1992) - A chemical model for generating the sources of mare basalts: Combined equilibrium and fractional crystallization of the lunar magmasphere. *Geochim. Cosmochim. Acta*, 56, 3809-3823, [https://doi.org/10.1016/0016-7037\(92\)90172-F](https://doi.org/10.1016/0016-7037(92)90172-F).
- Sprague A.L., Witterborn F.C., Kozlowski R.W., Cruikshank D.P., Bartholomew M.J., Graps A.L. (1992) - The Moon: Mid-infrared (7.5- to 11.4- μ m) spectroscopy of selected regions. *Icarus*, 100(1), 73-84, [https://doi.org/10.1016/0019-1035\(92\)90019-4](https://doi.org/10.1016/0019-1035(92)90019-4).
- Spudis P.D (1993) - The geology of multi-ring impact basin, The Moon and other planets. Cambridge University Press, Cambridge, UK, 131-164.
- [Stöffler D. and Ryder. G. \(2001\) - Stratigraphy and isotope ages of Lunar geologic units: Chronological standard for the Inner Solar System. In Kallenbach R., Geiss J., Hartmann W.K. \(Eds\), Chronology and evolution of Mars. Space Sci. Rev., 12, 9-54., \[https://doi.org/10.1007/978-94-017-1035-0_2\]\(https://doi.org/10.1007/978-94-017-1035-0_2\).](#)
- Stopar J.D., Robinson M.S., Barnouin O.S., McEwen A.S., Speyerer E.J., Henriksen M.R., Sutton S.S. (2017) - Relative depths of simple craters and the nature of the lunar regolith. *Icarus*, 298, 34-48. <https://doi.org/10.1016/j.icarus.2017.05.022>.
- Taylor L.A., Pieters C., Patchen A., Taylor D.H.S., Morris R.V., Keller L.P., McKay D.S. (2010) - Mineralogical and chemical characterization of lunar highland soils: Insights into the space weathering of soils on airless bodies. *J. Geophys. Res.*, 115, E02002, <https://doi.org/10.1029/2009JE003427>.
- Terada K., Morota T., Kato M. (2020) - Asteroid shower on the Earth-Moon system immediately before the Cryogenian period revealed by KAGUYA. *Nat. Comm.*, 11(1), 3453.
- Tobler W. (1987) - Measuring spatial resolution. Proceedings of the Land Resource Information Systems Conference, 48(January 1987), 12-16
- Warell J., Sprague A.L., Emery J., Long A. (2004) - Moon: First spectra from 0.7 to 5.5 μ m. *Lunar Planet. Sci.*, XXXV, 1624.
- Warren P.H. and Wasson J.T. (1979) - The origin of KREEP. *Rev. Geophys.*, 17(1), 73-88.
- Warren P.H. (1985) - The magma ocean concept and lunar evolution. *Ann. Rev. Earth Planet. Sci.*, 13(1), 201-240.
- Wellsz E. and Hapke B. (1977) - Lunar soil: Iron and titanium bands in the glass fraction. *Science*, 195, 977-979.
- Wilhelms D.E. and Davis D.E., (1971) - Two former faces of the Moon. *Icarus*, 15, 368-372.
- Wood C.A. and Andersson L. (1978) - New morphometric data for fresh lunar craters. *Icarus*, 20, 503-506.
- Wu B., Li F., Ye L., Qiao S., Huang J., Wu X., Zhang H. (2014) - Topographic modeling and analysis of the landing site of Chang'E-3 on the Moon. *Earth Planet. Sci. Lett.*, 405, 257-73, <https://doi.org/10.1016/j.epsl.2014.09.009>.
- [Wu W., Li C., Zuo W., Zhang H., Liu J., Wen W., Su Y., Ren X., Yan J., Yu D., Dong G. \(2019\) - Lunar Farside to be explored by Chang'e-4. Nat. Geosci., 12\(4\), 222-23, <https://doi.org/10.1038/s41561-019-0341-7>.](#)
- [Xu X., Hui H., Chen W., Huang S., Neal C.R., Xu X. \(2020\) - Formation of Lunar highlands anorthosites. Earth Planet. Sci. Lett., 536, 116138, <https://doi.org/10.1016/j.epsl.2020.116138>.](#)
- Yamamoto S., Nakamura R., Matsunaga T., Ogawa Y., Ishihara Y., Morota T., Hirata N., Ohtake M., Hiroi T., Yokota Y., Haruyama J. (2010) - Global distribution of olivine exposures on the Moon revealed by SELENE Spectral Profiler. *Lunar Planet. Sci.*, XXXII, 1646.

Manuscript received 20 April 2023; accepted 28 July 2023; published online XX November 2023; editorial responsibility and handling by M. Pantalonì.